Modeling of crazing using a cohesive surface methodology

Tijssens, M.G.A.; van der Giessen, E.; Sluys, B.L.J.

Published in:
Mechanics of Materials

DOI:
10.1016/S0167-6636(99)00044-7

Publication date:
2000

ELSEVIER

Mechanics of Materials 32 (2000) 19–35

MECHANICS OF MATERIALS

www.elsevier.com/locate/mechmat

Modeling of crazing using a cohesive surface methodology

M.G.A. Tijssens, E. van der Giessen *, L.J. Sluys

Delft University of Technology, Stevinweg 1, 2628 CN Delft, The Netherlands

Received 2 March 1999; received in revised form 12 July 1999

Abstract

A novel cohesive surface model for crazing in polymers is developed. The model incorporates the initiation, growth and breakdown of crazes based on micromechanical considerations. The initiation of crazes is controlled by the stress state, in particular by the hydrostatic stress and cohesive surface normal traction. The widening of a craze is based on a rate-dependent viscoplastic formulation and failure of the craze occurs when the fibrils reach a material-dependent maximum extension. Crazing is simulated using a high density of cohesive surfaces immersed in the continuum. The finite element method is used to discretize both cohesive surfaces and continuum separately. The capabilities of the method to describe multiple crazing is demonstrated with an example.

Keywords: Cohesive surface; Crazing; Polymers; Viscoplastic; Finite element

1. Introduction

Polymers typically exhibit two types of failure: shear yielding and crazing. In contrast to shear yielding, which results in relatively high energy dissipation, crazing is often the precursor to brittle fracture. Under special conditions, such as compressive loading, both thermoplastics and thermosets can be made to shear yield, but under tension many polymers fail in a brittle manner. Polymer blends are systems in which a dispersion of small rubber particles has been added with the intent to toughen the material by suppressing crazing and promoting shear yielding. In many blends, such as high impact polystyrene (HIPS) and acrylonitrile–butadien–styrene (ABS), crazing and shear yielding occur simultaneously. In these materials as well as in composites, multiple crazing occurs and is controlled by the microstructure. The way in which crazing initiates and propagates through these heterogeneous systems is however largely unknown.

In the past decades, research concerning the initiation and widening of crazes has contributed much to our understanding of the crazing phenomenon. Excellent reviews on the physical processes underlying the crazing of polymers have been given by Kramer (1983) and Kramer and Berger (1990). Three stages are often identified: initiation, propagation and widening. Sternstein et al. (1968) performed experiments on perforated strips of PMMA to explore the crazing behavior in a well-defined stress field. By comparing the regions in which no crazing was observed with the elastic solution for the stress field around a circular hole, they derived conditions for the stresses to be

* Corresponding author. Tel.: +31-15-278-65-00; fax: +31-15-278-21-50.

E-mail address: e.vandergiessen@wbmt.tudelft.nl (E. van der Giessen)

0167-6636/00/$ - see front matter
PII: S0167-6636(99)00044-7

fulfilled for crazing to occur. This initiation criterion for crazing was further explored by Sternstein and Myers (1973) close to biaxial stress states. A more mechanism-based approach was adopted by Argon (1973b) who presented a model for crazing based on the thermally activated expansion of pores. Argon and Hannoosh (1977) later revised this model and applied it to the initiation of crazes in polystyrene. At present there is no consensus on a general criterion for craze initiation.

Also, the propagation of the craze front is still a topic of debate. Argon and Salama (1977) proposed the meniscus-instability model for the longitudinal expansion of the craze. The model is justified by the observation that a model based on the continuous nucleation of micropores would give a closed-cellular craze structure, which is not consistent with the craze topology that is often observed experimentally, i.e., a structure through which air and fluids can be freely transmitted. Experimental evidence for this propagation mechanism is given by Donald and Kramer (1981), while the concept has been adopted, for instance, by Spiegelberg et al. (1991) and Kotoul (1996) to rationalize craze propagation properties. However, Argon and Salama (1977) recognize that for stress levels above roughly 0.4 to 0.5 times the material yield stress, the propagation mechanism of repeated void nucleation is well suited to predict craze propagation. Crazes that initiate under such stress state do exhibit the closed-cellular structure.

The third basic phenomenon during crazing is the widening of an existing craze in a direction normal to its 'plane'. In contrast to the aforementioned longitudinal expansion of the craze tip, there does seem to be consensus that the widening of a craze is to a large extent determined by surface drawing. This is the mechanism whereby the craze widens by continuously pulling new polymer material into the craze structure. There is direct experimental evidence for this, but the role of a number of suggested kinetic steps is not clear. A few first models for craze widening exist in the literature (Kramer, 1983; Leonov and Brown, 1992) but they leave much room for further improvement.

The numerical simulation of crazing has been undertaken at various length scales. At the molecular level, Han et al. (1998) developed a model to describe the strain rate effect on the surface energy and crazing mechanisms in fairly low molecular weight polymers. On a somewhat larger scale of observation, Sha et al. (1997) used a spring network model to explicitly model the fibrils in the craze. They related the critical craze width and fracture toughness of the craze to the microstructure of the craze and showed the important influence of the cross-tie fibrils on the total lifetime of the craze. At the continuum level, Brown (1991) proposed a uniform strip model in which the craze is modeled as a thin anisotropic elastic continuum of uniform thickness loaded by the application of a uniform displacement on the strip boundary. Xiao and Curtin (1995) also used a spring network model to describe the process of crazing. Based on rather simple rules, they transformed 'continuum springs' into 'craze springs', thus simulating craze initiation and development self-consistently, i.e., without a separate criterion for craze front propagation. Qualitatively, several experimental observations on craze growth were reproduced, such as a constant stress along the outer boundary of the craze and the simultaneous widening and propagation of the craze. There have also been a few attempts to describe a craze by a Dugdale-like, so-called cohesive surface (e.g., Döll et al., 1980). Within such a framework, Knauss (1993) explored the influence of different cohesive traction laws on crack stability.

In previous models of crazing, the constitutive behavior of the craze material has been rather much simplified. For example, Sha et al. (1997) and Brown (1991) have assumed the craze material to be purely elastic, while the rate-dependence incorporated by Knauss (1993) is limited to nonlinear viscoelastic behavior. However, an important toughening mechanism is neglected in such an approach, since the transformation of bulk polymer in crazed material must be accompanied by significant plastic deformation.

Also the use of cohesive surfaces so far often has been restricted to predetermined crack paths. Although useful to describe brittle crack propagation by a single dominating craze, this does not allow for the study of multiple crazing in heterogeneous polymer-based systems. The model that is

proposed in this paper aims at a description of crazing with cohesive surfaces that is suitable for studying massive crazing in, for instance, amorphous polymer–rubber blends. It borrows the original idea of Xu and Needleman (1994) to embed cohesive surfaces within a finite element discretization of a continuum. The constitutive model for each cohesive surface is based on micromechanical considerations of the (i) initiation, (ii) widening and (iii) breakdown of crazes in amorphous polymers, though in this paper we will focus mainly on the first two topics. The motivation for the model and its formulation will be outlined in the following sections, along with the numerical implementation. The simulation of crazing around a circular hole in an elastic plate subject to plane stress conditions, similar to the experiments done by Sternstein et al. (1968), will be used to illustrate the capabilities of the formulation.

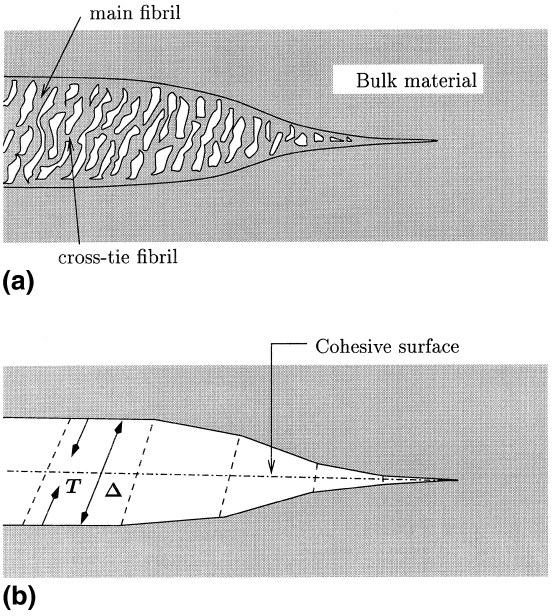

Fig. 1. Schematic of modeling a craze (a) by a cohesive surface (b) characterized by a traction $\boldsymbol{T}$ and a separation $\boldsymbol{\Delta}$ over this surface.

2. Formulation

2.1. Cohesive surface idealization for crazes

Crazes in amorphous polymers generally reach lengths in the order of tenths of millimeters, whereas the width of the craze remains in the order of several micrometers. Crazes in semicrystalline polymers such as polyethylene can become substantially wider but that involves additional mechanisms that are not taking place in the amorphous polymers that we focus on here. Neglecting the thickness of the craze, one can replace a craze by a cohesive surface, as illustrated in Fig. 1 where the length dimension is scaled down for illustrative purposes. The separation between two initially adjacent material points, one situated in the upper bulk–craze interface and the other in the bottom bulk–craze interface is described by a separation vector $\boldsymbol{\Delta}$ with normal component Δ_n and tangential component Δ_t with respect to the midplane of the cohesive surface, as illustrated in Fig. 2. The traction vector $\boldsymbol{T}$ is energetically conjugate to $\boldsymbol{\Delta}$ and has components T_n and T_t. The properties of the craze matter are thus collapsed in the traction vs separation law, which will be specified below.

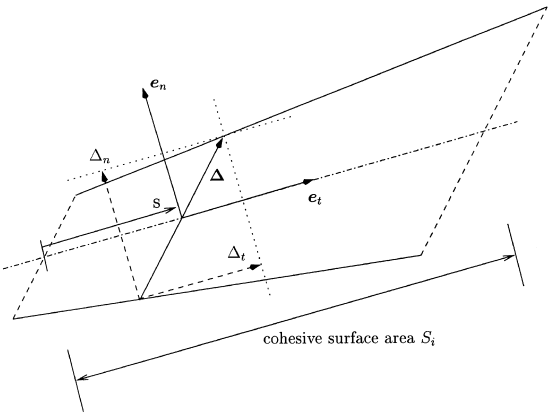

Fig. 2. Geometry of a cohesive surface with local basis $\{\boldsymbol{e}_n, \boldsymbol{e}_t\}$.

Multiple crazing in heterogeneous materials can be represented by embedding many potential cohesive surfaces throughout the volume. The constitutive behavior of the bulk material and the craze matter are thus separated by separate constitutive laws for the cohesive surfaces and for the continuum. Focusing attention here on brittle polymers with no other mechanism for inelastic

behavior than crazing, we describe the bulk continuum simply by Hooke's law. Crack propagation and fracture of the material as a whole then becomes independent of criteria for crack advance and only based on the description of the crazing process in the cohesive traction–separation law. The embedding of cohesive surfaces in a continuum was first introduced by Xu and Needleman (1994) in the context of brittle, rate-independent fracture, but without recourse to a particular fracture mechanism.

The constitutive model for cohesive surfaces for crazing should incorporate (at least): (i) the initiation, (ii) the widening and (iii) the eventual breakdown of the craze material. These will be presented consecutively.

2.2. Craze initiation

The physical mechanism for craze initiation is not yet clearly understood and multiple criteria have been proposed according to the assumed mechanism and the length scale of its description (see Kausch, 1987, for an overview). Experimentally (e.g., Argon and Hannoosh, 1977), when a constant stress is applied, an induction time for craze formation and a saturation of the total number of craze nucleation sites are observed. As the level of loading increases, the delay time for craze nucleation decreases while the amount of craze sites at saturation increases, indicating that craze initiation is a rate and stress-dependent phenomenon.

Argon and Salama (1977) showed that for stress levels above 0.4 to 0.5 times the material yield stress, craze initiation is well predicted by assuming a mechanism of repeated void nucleation. Furthermore, such stress levels involve an induction time of craze initiation that is almost negligible since the material is 'very rapidly' (Argon and Salama, 1977) filled by craze initiation sites.

In the present description, we choose to neglect the time delay for craze initiation. We consider that craze initiation is an instantaneous process which arises when, locally, a critical stress state is reached. Note that the cohesive surface formulation is flexible enough to account for more complex craze initiation criteria once such criteria become available. We shall now compare two of such stress state-dependent craze initiation criteria: the one given by Sternstein et al. (1968) and the criterion according to Argon and Hannoosh (1977).

The first criterion was derived from experiments on thin PMMA strips with a hole in the center to obtain a well-defined nonuniform stress field. Applying a far-field uniaxial tensile stress and recording the regions in which crazing occurred, Sternstein et al. (1968) deduced the following requirements for crazing to occur: (i) the hydrostatic stress must be positive and (ii) there exists a threshold value for the maximum principal stress below which craze initiation does not occur. On the basis of this, Sternstein and Myers (1973) formulated that crazing occurs once the following condition is satisfied:

$$|\sigma_1 - \sigma_2| \geqslant -A + \frac{B}{I_1}, \tag{1}$$

in which σ_1 and σ_2 are the maximum and minimum principal stresses, respectively, $A > 0$ and $B > 0$ are temperature-dependent constants and $I_1 = \sigma_1 + \sigma_2$ is three times the hydrostatic stress under plane stress conditions (note that A was called $-A$ in Sternstein and Myers, 1973). We shall interpret the corresponding equality to be the craze initiation criterion. Sternstein and Myers (1973) also give experimental values for the parameters A and B for PMMA as a function of temperature T. Following Argon (1973b) in the assumption that craze nucleation is a thermally activated process, we will assume that the parameters $A(T)$ and $B(T)$ vary with temperature according to an Arrhenius expression,

$$\begin{aligned} A(T) &= A(0)\ \exp(Q_a/kT), \\ B(T) &= B(0)\ \exp(Q_b/kT), \end{aligned} \tag{2}$$

in which k is Boltzmann's constant and $A(0)$, $B(0)$, Q_a and Q_b must be determined from experimental data. Interpolation of the data given in Sternstein and Myers (1973) with (2) results in a correlation coefficient of $r = 0.998$. Using, instead a linear temperature dependence, we find a slightly worse correlation: $r = 0.98$. The extrapolation of the values of $A(T)$ and $B(T)$ over relatively large

temperature intervals when using a linear relation or the exponential relation (2) can lead to large differences; but, the exponential extrapolation is physically better motivated and therefore we will continue to use that. From the experimental data for PMMA given by Sternstein and Myers (1973), we calculate $A(0) = 0.0253$ MPa, $B(0) = 4.402\times 10^{-3}$ MPa^2, $Q_a/k = 2322$ K and $Q_b/k = 4205$ K. This results in values for $A(T)$ and $B(T)$ at room temperature ($T = 293$ K) of $A = 70$ MPa and $B = 7500$ MPa^2.

The criterion given by Argon and Hannoosh (1977) is based on the work of Argon (1973a) in which a craze initiation process is proposed that consists of two stages. First, microshear bands will deform the polymer material on the molecular level, causing the local pore density to increase as these microshear bands get arrested by molecular level plastic heterogeneities. Once a critical stress level and porosity is reached, plastic cavitation becomes possible and a craze nucleus is formed. A thermodynamic consideration then lead Argon and Hannoosh (1977) to conclude that craze initiation takes place once the condition

$$\frac{(A^1/SQ)}{(\xi/Q)} - (\xi/Q) - \ln\left[1 - \left(\frac{\beta}{\xi/Q}\right)^m\right] = C \qquad (3)$$

is satisfied. Here, $A^1 = 9.545$, $C = 21.23$, and $Q = 0.0133$ are constants given in Argon and Hannoosh (1977) which have been determined from experiments on crazing in polystyrene, and $m = 24$, $\beta = 0.6$ result from the assumptions and substitutions made in the derivation. For the case of a perfectly smooth surface, the variable S is given by

$$S = \sqrt{\frac{1}{3} + (\eta/\xi)^2} \qquad (4)$$

in terms of the dimensionless hydrostatic stress and effective stress $\xi = (\sigma_1 + \sigma_2)/2Y$ and $\eta = (\sigma_1 - \sigma_2)/2Y$, respectively, where Y is the bulk yield stress of the polymer.

The stress dependencies in both craze initiation criteria are distinctly different. Unfortunately, the two criteria have been validated on two different materials, PS vs PMMA, so that a quantitative comparison is not possible. However, it is of interest to compare the criteria in a qualitative manner. To that end, we first rewrite the Sternstein criterion (1) for craze initiation in terms of ξ and η as

$$|\xi| + \frac{A}{2Y} - \frac{B}{(2Y)^2\eta} = 0. \qquad (5)$$

Both criteria are plotted in Fig. 3, assuming the values of A and B for PMMA at room temperature given previously and estimating the yield stress Y of PMMA between 100 and 120 MPa. It seems that both criteria determine craze initiation to occur at similar stress states, except in the region of low hydrostatic stresses. Because of the lack of consensus about craze initiation criteria and the relative simplicity of the Sternstein criterion (1), this criterion will be used for illustration purposes in this paper. However, the methodology is sufficiently flexible to allow for other criteria.

Both criteria, as well as others, involve two crucial stress components for craze initiation, viz., the hydrostatic stress σ_m and the maximum principle stress σ_1. For use in the cohesive surface methodology, the initiation criterion must be rewritten in terms of, primarily, the components of the traction vector $\boldsymbol{T}$ and other stress state characteristics when necessary. We will discuss this

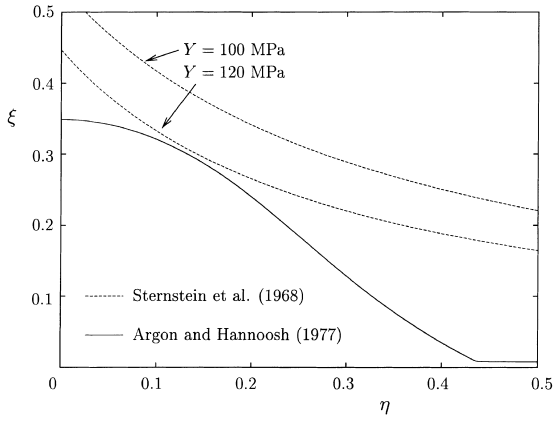

Fig. 3. The initiation criteria for crazing at room temperature ($T = 293$ K), plotted as a function of effective stress $\eta = (\sigma_1 - \sigma_2)/2Y$ and hydrostatic stress $\xi = (\sigma_1 + \sigma_2)/2Y$ according to Argon and Hannoosh (1977) for PS (see (3)) and Sternstein et al. (1968) for PMMA (see (1) or (5), $A = 70$ MPa, $B = 7500$ MPa^2).

here for the Sternstein criterion, noting that it was based on plane stress experiments for which the hydrostatic stress is given by $\sigma_m = (1/3)(\sigma_1 + \sigma_2)$. Assuming the maximum principal stress σ_1 to be equal to the normal traction component T_n, we can write $\sigma_2 = 3\sigma_m - T_n$. Using this to eliminate σ_1 and σ_2, the initiation criterion of Sternstein (1) takes the form

$$f(T_n, \sigma_m) = \frac{3}{2}\sigma_m - \frac{1}{2}A + \frac{B}{6\sigma_m} - T_n = 0. \tag{6}$$

The region $f < 0$ in $\sigma_m - T_n$ space signifies the stress states that are not accessible without triggering crazing. It is straightforward to rewrite the Argon–Hannoosh criterion (3) in a similar fashion. Both criteria have been plotted in $\sigma_m - T_n$ space in Fig. 4. The region of interest in Fig. 4 is limited by the conditions,

$$T_n = \sigma_1 > \sigma_2 = \alpha\sigma_1 \quad \text{and} \quad \sigma_m = \frac{1}{3}(1+\alpha)\sigma_1 > 0, \tag{7}$$

where $\alpha < 1$. Hence, only the region $0 < \sigma_m < \frac{2}{3}T_n$ is of interest. It is seen in this figure, that the Argon–Hannoosh criterion is practically equivalent to a constant normal stress criterion over a relatively wide range of mean stresses. By contrast, the influence of the hydrostatic stress is seen to be much more pronounced in the Sternstein criterion.

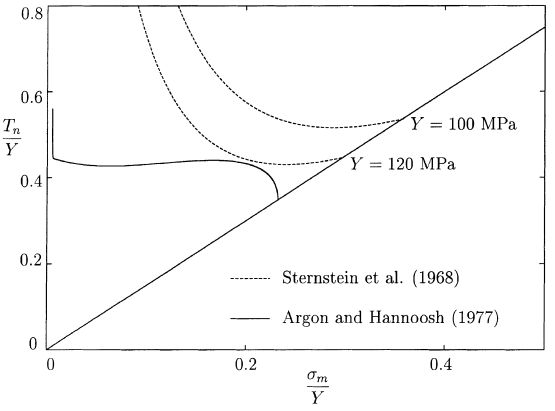

Fig. 4. The initiation criteria for crazing shown in Fig. 3, but replotted now as a function of the cohesive normal stress and the hydrostatic stress.

2.3. Craze widening

Once a craze has initiated, widening of the craze is assumed to be a process of drawing in new polymer material from the craze-bulk interface (Kramer, 1983; Kramer and Berger, 1990). This is illustrated schematically in Fig. 5. The highly stretched network of molecules in the fibrils strongly resists further elongation, thereby pulling new amorphous material into the fibril. As these fibrils continue to form, the initial craze 'voids' grow into highly prolate toroidal space around the fibrils. The stress at which new fibril material is drawn from the bulk material is often taken to be a material parameter. However, when originally amorphous polymer material is transformed into the highly stretched and oriented fibril material, this process must be governed by substantial plastic deformation of the polymer material and therefore must be strongly rate-dependent. A preliminary detailed study of this has been carried out by Van der Giessen and Lai (1997). Kramer and Berger (1990) have pointed out that chain scission and chain disentanglement are also important mechanisms of craze widening. However, these mechanisms have not been well-described so far. In view of the lack of complete detailed description of craze widening at this moment, we adopt here a rather phenomenological constitutive description that is inspired partly by the early qualitative analyses of Kramer and Berger (1990) and of Leonov and Brown (1992) and partly by the

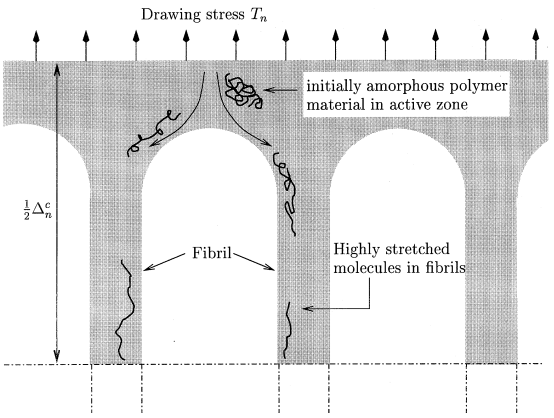

Fig. 5. Illustration of the surface drawing mechanism.

numerical results of the more quantitative study in Van der Giessen and Lai (1997). The basic assumption is that the viscoplastic flow into the fibrils is the rate-limiting process. In analogy with the description of rate-dependent plastic deformation in bulk glassy polymers according to Argon (1973a), we propose the following widening law in terms of the normal separation rate $\dot{\Delta}_n^c$ as a function of the normal stress T_n:

$$\dot{\Delta}_n^c = \dot{\Delta}_0 \exp\left[-\frac{A^*\sigma_c}{T}\left(1-\frac{T_n}{\sigma_c}\right)\right]. \tag{8}$$

Here, A^*, $\dot{\Delta}_0$, and σ_c are material constants; $\dot{\Delta}_0$ is the separation rate when T_n reaches values as high as σ_c; A^* governs a linear drop in normal traction T_n with temperature at a given separation $\dot{\Delta}_n^c$ and σ_c is the athermal stress for craze widening.

Craze material is a complex structure in which long cylindrical fibrils of polymer material are interconnected by cross-tie fibrils which give the craze some tangential load carrying capacity while it widens. In a cohesive surface representation we therefore need to account for a resistance against tangential separation in terms of a constitutive description of $\dot{\Delta}_t^c$ as a function of T_t. As the geometry of the craze material suggests a coupling between the tangential separation and the normal separation, we propose the following viscoplastic tangential separation law, similar to (8):

$$\dot{\Delta}_t^c = \dot{\Gamma}_0\left\{\exp\left[-\frac{A^*\tau_c}{T}\left(1-\frac{T_t}{\tau_c}\right)\right] - \exp\left[-\frac{A^*\tau_c}{T}\left(1+\frac{T_t}{\tau_c}\right)\right]\right\}, \tag{9}$$

in which $\dot{\Gamma}_0$ and τ_c are material parameters. Note that in contrast to the normal viscoplastic widening law (8) an extra term is included that is necessary to ensure that $\dot{\Delta}_t^c$ is an odd function of T_t.

Because of the expected coupling between tangential separation and normal separation due to widening of the craze, one would expect the material constants σ_c and τ_c and $\dot{\Delta}_0$ and $\dot{\Gamma}_0$, respectively, to be related. This relationship requires a detailed study of craze widening at a lower length scale than we consider here. This has not been investigated, to the authors' knowledge. Therefore, we here propose a heuristic relationship by identification of σ_c and τ_c and $\dot{\Delta}_0$ and $\dot{\Gamma}_0$, respectively, through the concepts of Von Mises effective stress and the conjugate effective strain rate: $\tau_c = \sigma_c/\sqrt{3}$ and $\dot{\Gamma}_0 = \sqrt{3}\dot{\Delta}_0$.

2.4. Craze breakdown

For a long time, widening of crazes was assumed to be the result of creep deformation of the fibrillar material. Breakdown of crazes was therefore assumed to occur at the mid rib of the craze, which is the oldest portion of the craze material. However, crazes have been shown to break down at the craze-bulk interface, see Kramer and Berger (1990), thus pointing to a mechanism in which imperfections such as dust inclusions are responsible for the eventual failure of the craze. More recently, considerable theoretical progress has been made in understanding the reason for craze breakdown. Brown (1991) was the first to point out the important role of the cross-tie fibrils as the cause for craze breakdown, and this was further quantified by Hui et al. (1992). Later, Sha et al. (1997) developed a detailed microstructural model of a craze and related the critical craze width and fracture toughness of the craze to its fibril network structure. They then showed the important influence of the cross-tie fibrils on the total lifetime of the craze.

Although it is now recognized that the cross-tie fibrils play a crucial role in the lifetime of a craze, the theoretical framework on craze breakdown is far from complete. The cited works all represent a craze on a smaller lengthscale then what we are searching for in our cohesive surface representation. In the latter, the influence of the cross-tie fibrils on craze breakdown should be taken into account through a dependence on the tangential cohesive separation mode. As pointed out in the previous section, this deformation mode is still far from being understood and detailed theoretical studies are needed to arrive at a satisfying description.

In our formulation, we therefore follow the results obtained through experiments, though the cohesive surface framework can be easily extended once more sophisticated theoretical models become available. According to Kramer and Berger (1990), the statistics of craze fibril breakdown have been found experimentally to follow a Weibull distribution with respect to the plastic strain in the craze. Nevertheless, experiments by Döll et al. (1979) show that the maximum craze opening at breakdown is constant over a wide range of crack tip velocities (from 10^{-8} to 20 mm/s). In the cohesive surface model, we therefore simply assume that craze breakdown occurs as soon as the plastic craze opening Δ_n^{c} attains a critical value $\Delta_n^{\mathrm{c,cr}}$ which is taken to be constant with respect to time, temperature and loading rate.

3. Numerical implementation

Confining attention here to polymers with bulk elastic properties, we do not expect large strains in the bulk polymer. However, finite strain effects may be of importance in the neighborhood of the crack tip, and will certainly be so when the cohesive surface models are to be used in the future for elastoplastic polymers. Therefore, we do account for finite strains in the continuum description, using a finite strain convected coordinate Lagrangian description. The material coordinates are the Cartesian coordinates in the undeformed configuration with basis $\boldsymbol{e}_i$, and the metric in the deformed state is denoted by G^{ij}. Elasticity of the bulk is incorporated through the well-known hypoelastic relation in terms of the Second Piola–Kirchhoff stress $\boldsymbol{\tau} = \tau^{ij}\boldsymbol{e}_i\boldsymbol{e}_j$ and the Lagrangian strain $\boldsymbol{\eta} = \eta_{ij}\boldsymbol{e}^i\boldsymbol{e}^j$:

$$\dot{\tau}^{ij} = \mathscr{L}^{ijkl}\dot{\eta}_{kl} \tag{10}$$

with $\mathscr{L}^{ijkl}$ the components of the material modulus tensor given by

$$\mathscr{L}^{ijkl} = \frac{E}{1+v}\left[\frac{1}{2}\left(G^{ik}G^{jl} + G^{jk}G^{il}\right) + \frac{v}{1-2v}G^{ij}G^{kl}\right] - \frac{1}{2}\left[G^{jk}\tau^{il} + G^{jl}\tau^{ik} + G^{il}\tau^{jk} + G^{ik}\tau^{jl}\right], \tag{11}$$

where E is Young's modulus and v is Poisson's ratio. The last bracketed term is the convective contribution that originates from the Jaumann stress rate used to ensure objectivity.

In the previous section, the constitutive description of crazes has been phrased in terms of rate equations (8) and (9) for the normal and tangential components $(\dot{\Delta}_n^{\mathrm{c}}, \dot{\Delta}_t^{\mathrm{c}})$ of the separation vector $\boldsymbol{\Delta}^{\mathrm{c}}$ due to crazing as strongly nonlinear functions of the traction components. For numerical convenience, we complete the constitutive law for the cohesive surfaces as

$$\dot{T}_\alpha = k_\alpha(\dot{\Delta}_\alpha - \dot{\Delta}_\alpha^{\mathrm{c}}), \quad \alpha = n, t. \tag{12}$$

Prior to craze initiation, the plastic widening rate of the craze vanishes, $\dot{\Delta}_\alpha^{\mathrm{c}} = 0$, and the stiffness k_α is purely artificial. The value needs to be high enough that the elastic deformation in the cohesive surfaces does not significantly alter the overall elastic properties. Once crazing has initiated, the stiffness k_α reflects the instantaneous elastic properties of the craze fibrils and part of the active material in the craze (see Fig. 1). The normal stiffness k_n can be estimated for instance from the numerical study in Van der Giessen and Lai (1997).

Although initially k_t must be sufficiently large for reasons mentioned before, after substantial widening the craze matter exhibits a low but finite tangential stiffness due to the cross-tie fibrils. For simplicity we here take the tangential stiffness to evolve with the craze width Δ_n^{c} from its initial value k_t^0 according to

$$k_t = k_t^0 \exp\left\{-c_1\frac{\Delta_n^{\mathrm{c}}}{\Delta_n^{\mathrm{c,cr}}}\right\} \tag{13}$$

so that the ultimate value at craze breakdown is $k_t = k_t^0 \exp(-c_1)$. This is illustrated in Fig. 6 for $c_1 = 10$ and $c_1 = 50$. Throughout our calculations we have used $c_1 = 50$.

The numerical solution of the equations is obtained using a linear incremental analysis within the finite element context. For each discrete time step Δt during the incremental procedure equilibrium is specified through the rate form of the principle of virtual work:

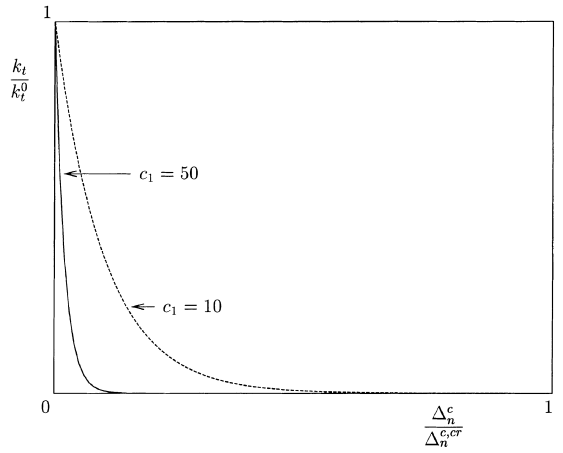

Fig. 6. Illustration of the decrease of the tangential stiffness as a function of the plastic craze opening Δ_n^c.

$$\Delta t \int_V \left(\dot{\tau}^{ij} \Delta \eta_{ij} + \tau^{ik} \dot{u}^j_{,k} \delta u_{j,i} \right) \mathrm{d}V + \Delta t \int_{S_i} \dot{T}_\alpha \delta \Delta_\alpha \, \mathrm{d}S = \Delta t \int_{S_u} \dot{t}^i \delta u_i \, \mathrm{d}S - \left[\int_V \tau^{ij} \delta \eta_{ij} \, \mathrm{d}V + \int_{S_i} T_\alpha \delta \Delta_\alpha \, \mathrm{d}S - \int_{S_u} t^i \delta u_i \, \mathrm{d}S \right], \tag{14}$$

in which V and S_u are the volume and outer surface of the body in the reference configuration and S_i is the current internal cohesive surface. The latter is the collection of all cohesive surface elements contained in V. They may be confined to a single surface in the material (if, for example, the craze location is known a priori) or may be scattered over the entire volume, as pioneered in Xu and Needleman (1994). The latter approach is what is used here in combination with linear triangular elements for the continuum. As illustrated in Fig. 7, this crossed-triangle arrangement provides the maximum freedom for the direction of the craze path.

The term in (14) between square brackets is the equilibrium correction which is zero for a state of perfect equilibrium. This term is included to prevent drifting of the solution from the true equilibrium path due to the finite time increments. The finite element equations are obtained by eliminating the stress rates $\dot{\tau}^{ij}$ using (10) and (11) and eliminating the cohesive surface traction rates

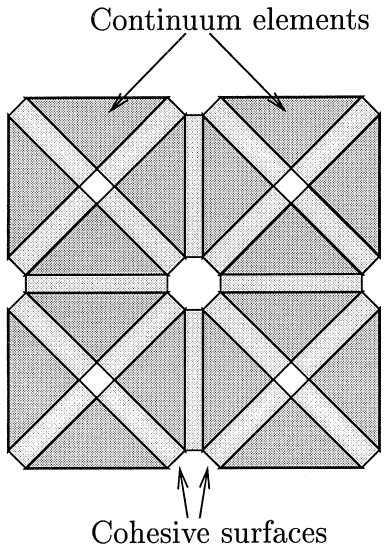

Fig. 7. Illustration of the arrangement of continuum elements and cohesive surfaces.

using (8), (9) and (12). As pointed out by Schellekens and De Borst (1993) the numerical integration of the stiffness contributions of the cohesive surface elements with Gauss quadrature may lead to numerical errors if traction gradients are large. In such cases the numerical integration is best carried out with Newton–Cotes integration. In this paper an example is given in which traction gradients remain low, so that a two-point Gauss scheme is justified.

It is of importance to note that the constitutive description of the cohesive surfaces for crazing not only involves the cohesive traction $\boldsymbol{T}$ but, in the craze initiation criterion (6), also the hydrostatic stress. This information is gathered for each cohesive element from the continuum stresses in the elements on either side of the cohesive element. The hydrostatic stress is computed from the Piola–Kirchhoff stresses according to $\sigma_m = 1/3\tau^{ij}G_{ij}$, in which density changes due to elastic strains are neglected since they will remain small.

To increase the numerical stability and accuracy of the integration of the cohesive surface constitutive equations we employ a forward gradient scheme (Peirce et al., 1984) similar to that used for a different cohesive surface model by Van der Giessen and Tvergaard (1989). The plastic

separation rate $\dot{\Delta}_\alpha^c$ during the increment Δt is expressed as a linear interpolation between its values at time t and time $t+\Delta t$ according to

$$\dot{\Delta}_\alpha^c = (1-\theta)\dot{\Delta}_\alpha^{c,(t)} + \theta\dot{\Delta}_\alpha^{c,(t+\Delta t)}, \quad \theta \in [0,1]. \tag{15}$$

When we estimate $\dot{\Delta}_\alpha^{c,(t+\Delta t)}$ from the Taylor expansion

$$\dot{\Delta}_\alpha^{c,(t+\Delta t)} = \dot{\Delta}_\alpha^{c,(t)} + \left.\frac{\partial \dot{\Delta}_\alpha^c}{\partial T_\alpha}\right|_{(t)} \dot{T}_\alpha \Delta t \tag{16}$$

and substitute this into (12), we can re-arrange the result to obtain

$$\dot{T}_\alpha = k_\alpha^*(\dot{\Delta}_\alpha - \dot{\Delta}_\alpha^c), \tag{17}$$

in which the stiffness k_α^* is defined by

$$k_\alpha^* = k_\alpha \Big/ \left(1 + k_\alpha \theta \frac{\partial \dot{\Delta}_\alpha^c}{\partial T_\alpha}\Delta t\right). \tag{18}$$

For the computations to be presented later, we have used $\theta = 0.5$.

The accuracy is further increased by using the exact solution for the increment of the normal traction, ΔT_n, which is obtained by substituting (8) into (12) with $\alpha = n$. Integrating the resulting equation over the time interval $[t, t+\Delta t]$ and invoking that the normal separation rate $\dot{\Delta}_n^c$ is constant during this increment, we obtain

$$\begin{aligned}\Delta T_n = -\frac{T}{A}\ln\Bigg\{&\left(1 - \frac{\dot{\Delta}_0}{\dot{\Delta}_n}\exp\left[-\frac{A}{T}(\sigma_c - T_n)\right]\right)\\ &\times \exp\left[-\frac{A}{T}k_n\dot{\Delta}_n\Delta t\right]\\ &+ \frac{\dot{\Delta}_0}{\dot{\Delta}_n}\exp\left[-\frac{A}{T}(\sigma_c - T_n)\right]\Bigg\}.\end{aligned} \tag{19}$$

Since the tangential separation is expected to remain relatively small and the exact solution is computationally expensive, we use the forward gradient updating for the tangential separation mode according to (12) and (17).

During the incremental solution procedure, an adaptive time stepping scheme is used to ensure accurate integration of the constitutive equations. The criteria for adaptation of the time step are based on (1) accurate initiation of crazes, (2) accurate integration of the stresses during softening and unloading and (3) a limited separation rate to prevent premature breakdown. The expected traction–separation history of a craze is shown schematically in Fig. 8 in which the regimes for which each criterion may be critical have been indicated. The initiation of crazes is determined by (6) for plane stress situations. When during the incremental procedure it is detected that

$$f(T_n, \sigma_m) \geqslant 0 \quad \text{and} \quad f(T_n + \beta\Delta T_n, \sigma_m + \beta\Delta\sigma_m) \leqslant 0, \tag{20}$$

then β is determined such that $f \equiv 0$ and the time step is adjusted accordingly in order to capture the instant of craze nucleation exactly. The second criterion limits the increments of normal cohesive stresses to a fraction of a characteristic stress level, for which we take the craze widening stress σ_c of (8). When unloading occurs in a cohesive element, the time step is reduced such that the elastic unloading of the craze is completed within a few increments. To prevent very large time steps during the plateau of the craze traction and subsequent premature breakdown of the craze, the increments in separation are limited to a fraction of the maximum plastic craze opening. The numerical values of the margins used read:

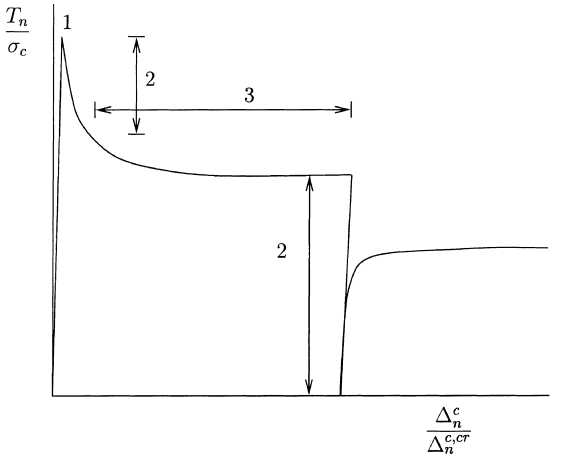

Fig. 8. Schematic traction–separation history of a craze. The numbers (see Section 3) indicate regions where various time stepping criteria are critical.

$$\frac{\Delta T_n}{\sigma_c} < 10^{-2}, \quad \dot{\Delta}_n < 10^{-1}\frac{\sigma_c}{k_n \Delta t}, \quad \dot{\Delta}_n < 10^{-2}\frac{\Delta_n^{c,cr}}{\Delta t}. \tag{21}$$

4. Application: crazing around a circular hole

To illustrate the capabilities of the proposed model to describe distributed crazing under inhomogeneous stress fields, we have carried out simulations of the problem used in the experimental work by Sternstein et al. (1968) to substantiate their initiation criterion. They investigated a strip of PMMA of length $2h = 2$ in., width $2b = 1/2$ in. and thickness $t = 1/32$ in. having a center hole with a diameter of $2R = 1/16$ in. The strip was loaded at a temperature of 343 K and a tensile stress of up to 4000 psi (27.6 MPa). The load was applied within a few seconds and thereafter kept constant.

4.1. Problem formulation

In the calculations we use a mesh as shown in Fig. 9. Symmetry is used along the axes x_1 and x_2. Fig. 9(b) shows the region in which cohesive surfaces are used. To reduce the computational effort, cohesive surfaces are limited to a segment of the circular region next to the equator of the hole. Each side of the triangular elements is connected to a cohesive surface as illustrated in Fig. 7.

The width, height and thickness of the plate are as specified above. The boundary conditions are given by

$$\begin{aligned}
&\text{at } x_1 = 0: \quad \dot{u}_1 = 0, \quad \dot{t}^2 = 0;\\
&\text{at } x_1 = b: \quad \dot{t}^1 = 0, \quad \dot{t}^2 = 0;\\
&\text{at } x_2 = 0: \quad \dot{u}_2 = 0, \quad \dot{t}^1 = 0;\\
&\text{at } x_2 = h: \quad \dot{t}^1 = 0, \quad \dot{t}^2 = \dot{p}.
\end{aligned}$$

Sternstein et al. (1968) did not specify the loading rate: the load was applied (quote) "in the matter of a few seconds". The applied traction rate $\dot{p}$ at the upper boundary is therefore specified by assuming that in the experiments the loading is applied within a time span of 2.5 or 5 s. For a final stress level of 27.6 MPa, this results in a rate of 11.0 MPa/s or of 5.52 MPa/s. The elastic properties are taken as $E = 3240$ MPa and $\nu = 0.35$.

Because of lack of experimental data, we assume the parameter A^* in the craze widening law (8) to be equal in value to what Arruda et al.

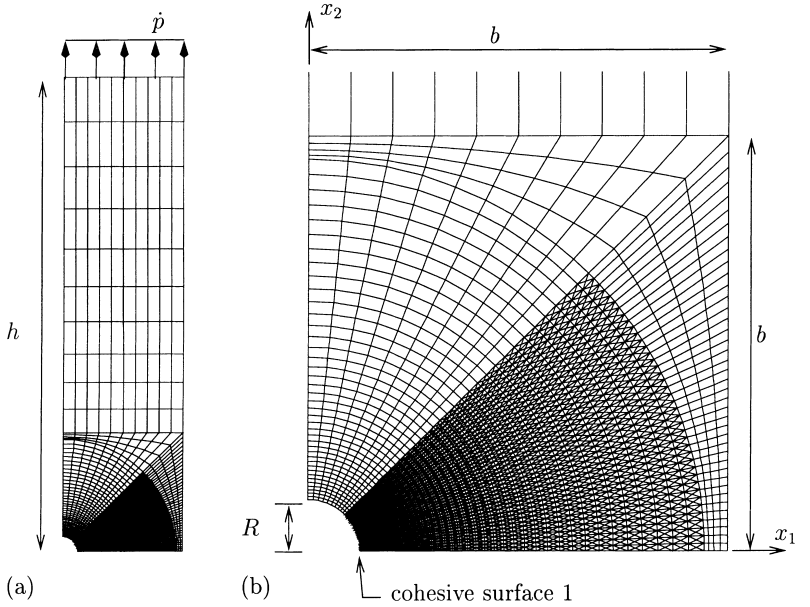

Fig. 9. Finite element mesh used for a quarter of the plate: (a) complete mesh; (b) detailed mesh with cohesive surfaces.

(1995) give for shear yielding of PMMA (i.e., $A^* = 101$ K/MPa). This implies that the temperature dependence of craze widening is equal to that of bulk viscoplasticity. From the experimental data of Döll et al. (1979), we find $\Delta_n^{c,cr} = 2.7$ μm. Although there is no conclusive experimental or numerical evidence, one generally assumes that crazes show softening after initiation, followed by a period of constant drawing stress, see e.g., Knauss (1993), Telenkov et al. (1998), and Warren (1989). The parameters $\dot{\Delta}_0 = 10$ mm/s and $\sigma_c = 60$ MPa are chosen such that for the loading rates and temperature range used in our calculations, the resulting traction–separation response of the crazes exhibits softening.

The stiffness k_α in (12) must be properly chosen so that the response prior to craze nucleation is not significantly affected by the presence of the cohesive surfaces. This is particularly important for applications like the present one where cohesive surfaces are immersed through the continuum element mesh. The ratio of the stiffness of the continuum elements and of the cohesive surface elements is approximately $E/(k_\alpha l)$, where l is a characteristic cohesive surface length. In our calculations, k_α is determined from $k_\alpha = \mu E/\Delta_n^{c,cr}$, where μ is adjusted such that $E/(k_n l) \leqslant 0.01$. The used value of k_n is also consistent with the results in Van der Giessen and Lai (1997).

4.2. Numerical results

The development of crazing around the hole has been studied over a range of 50 K, starting at room temperature ($T = 293$ K). Although there is practically no influence on the overall load–displacement curve, the region inside of which crazes are formed (the craze zone) depends quite sensitively on temperature. This is demonstrated in Fig. 10 for $T = 313$ and 333 K, at the loading rate of $\dot{p} = 5.52$ MPa/s. Crazing initiates in both cases from the equator of the hole, but at different instants since the critical stress for craze initiation is temperature-dependent. The crazing proceeds by propagation away from the hole and by simultaneous expansion in the loading direction. Thus, craze zones develop inside of which craze initiation has taken place in essentially all cohesive elements.

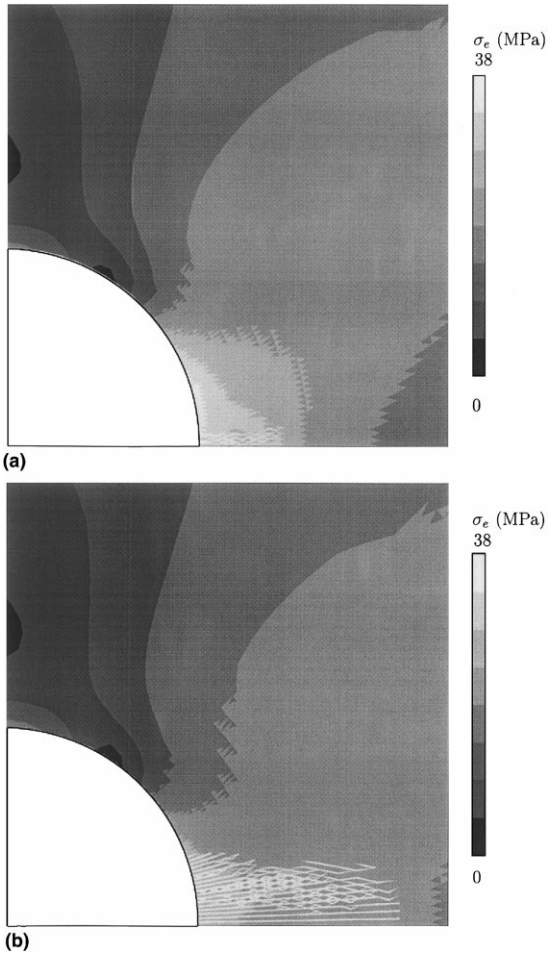

Fig. 10. Craze zone and effective stress distribution near the hole at a global stress level of $p = 16$ MPa for the case of $\dot{p} = 5.52$ MPa/s at (a) $T = 313$ K and (b) $T = 333$ K. The white 'fringes' in the neighborhood of the equator of the hole are the opened-up cohesive surface elements accounting for crazing.

At higher temperature, however, the craze zone at the same applied load level has propagated significantly further into the plate and is also substantially wider. The different craze zones that have developed also affect the stress distribution in the neighborhood of the hole.

In order to explain how this temperature dependence originates from the cohesive surface modeling, Fig. 11 provides a detailed view of the craze evolution at an integration point of a typical cohesive surface (cohesive surface number #1 indicated in Fig. 9) over the entire temperature

range. In the cohesive surface formulation proposed here, temperature affects both craze initiation and craze widening, and through these has an indirect influence on craze propagation. The assumed temperature dependence of the initiation parameters $A(T)$ and $B(T)$ given in (2) results in a rather strong increase of the normal traction on the cohesive surface at craze initiation with decreasing temperature, as is seen in Fig. 11(a). After craze initiation, the craze width evolves according to (8) where the temperature dependence stems from the prefactor $-A^*\sigma_c/T$. For the material parameters chosen here, the asymptotic plateau stress for craze widening is seen to be significantly less sensitive to temperature than the initiation stresses: roughly 5% lower than the craze initiation stress at $T = 323$ K increasing up to roughly 30% at $T = 293$ K.

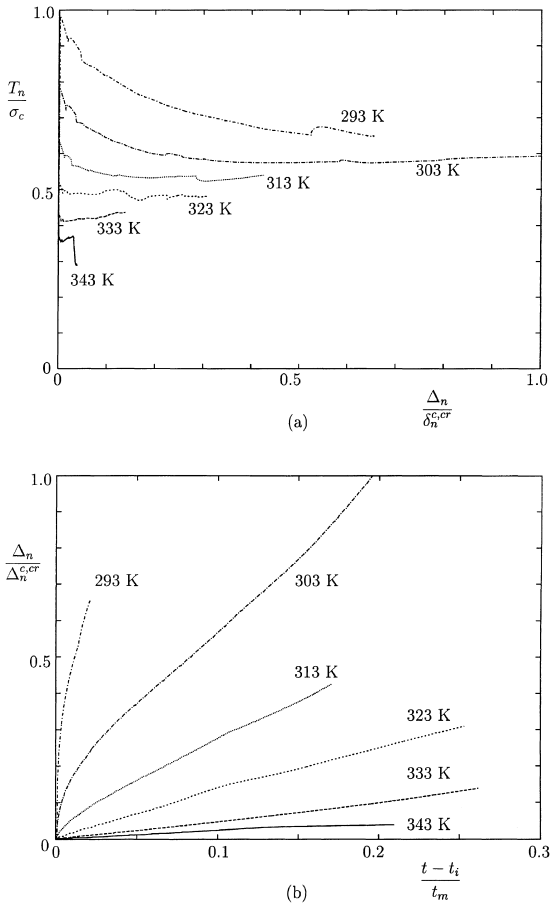

Fig. 11. Influence of temperature on the behavior of crazes at a loading rate of $\dot{p} = 5.52$ MPa/s. Normal cohesive traction as a function of normal separation (a) and normal separation as a function of the elapsed time $t - t_i$ after craze initiation (b) for different temperatures. Time to maximum load application $t_m = 5$ s.

It should be realized in interpreting these results that they are the result of a coupled problem involving growth and propagation of existing crazes as well as initiation of new ones, both in competition with stress relaxation in the undamaged bulk. Therefore, Fig. 11(b) additionally shows the evolution of the craze width in time at various temperatures. In order to compare the different cases, in which crazing has initiated at different instants t_i, the time evolution is plotted relative to t_i. Clearly, temperature has a dramatic effect on craze widening. At relatively low temperatures, the craze widens very rapidly while it behaves in a much more viscous manner at a 50° higher temperature. This must be attributed mainly to the different stress levels at the various temperatures, Fig. 11(a), which overrules the opposite effect of temperature in (8). As the critical craze opening for breakdown, $\Delta_n^{c,cr}$, is assumed independent of temperature, the results in Fig. 11(b) immediately indicate that breakdown will occur faster at lower temperatures, thus yielding more brittle behavior. A slightly more intricate consequence of this temperature dependence is that, since a craze widens slower as temperature increases, more crazes tend be initiated. This indicates that a more spread-out craze zone will develop at higher temperatures, which agrees with the results in Fig. 10.

In the present formulation, craze initiation is rate independent but rate effects are included in craze widening. Their influence is briefly investigated in Fig. 12 by comparing results for the default loading rate with a two times higher rate. Again, the net effect at an individual craze is the consequence of the competing processes. An increase in widening rate at a higher loading rate requires a higher cohesive normal stress, according to (8), but that tends to enhance the initiation of new crazes, which reduces the local strain rate. The net effect for the point at the craze considered here is that the craze normal stress is hardly affected by the loading rate, Fig. 12(a), while as a consequence

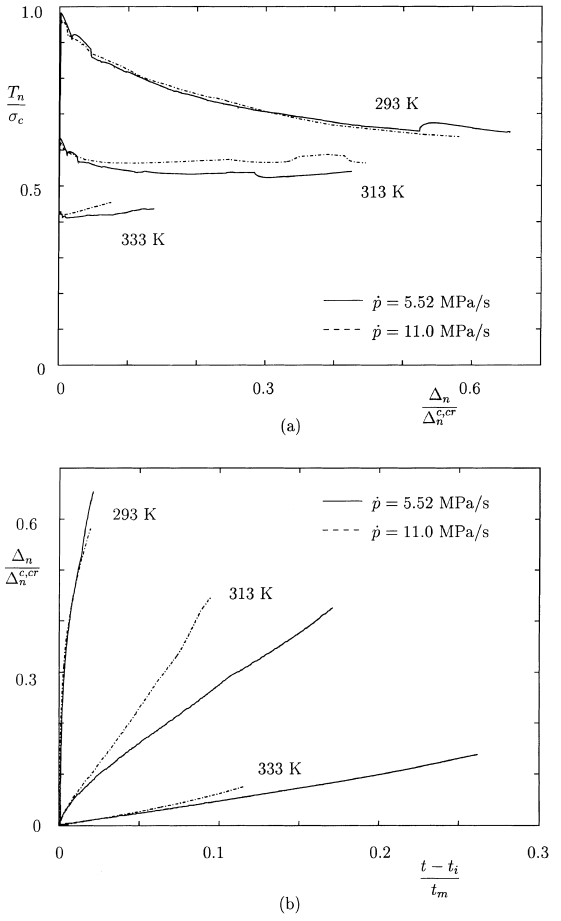

Fig. 12. Influence of loading rate on the behavior of crazes. Normal cohesive traction as a function of normal separation (a) and normal separation as a function of the elapsed time $t - t_i$ after craze initiation (b) for different loading rates. Normalizing factor $t_m = 5$ s.

of the nonlinear response, the opening rate does tend to be accelerated. The latter is indicative of a more brittle response at a higher loading rate.

It is observed from Fig. 10 that crazes develop more or less in the maximum principal stress direction of the elastic solution around a hole (see, e.g., Timoshenko and Goodier (1951). This is in qualitative agreement with the common, albeit imprecise, viewpoints in the polymer community (Kausch, 1987). Sternstein et al. (1968) deduced their criterion for craze initiation by comparing the craze zone development with the analytical solution for the stress field around a circular hole. In particular, they focused on the behavior near the poles of the hole, noting that the theoretical contours are (quote) "a good first approximation to the stresses in this region" as no crazing occurs there. They also point out that the elastic solution may *not* be representative in the region near the equator of the hole. This is explored in Fig. 13, which depicts the craze zone development with increasing load for the case of $\dot{p} = 5.52$ MPa/s at $T = 333$ K. The elastic prediction for the craze zone was calculated by substituting the solution for the elastic stress field into (1). We see that the predicted craze zone has a significantly different shape than that predicted by the unperturbed elastic solution. The difference between the two is further evidence of the stress re-distributions taking place during crazing, as seen already in Fig. 10.

It is worth noting that until the instant shown in snapshot #6 in Fig. 13, craze breakdown has not occurred anywhere. Hence, stress is still being transmitted across the craze zone, albeit limited by

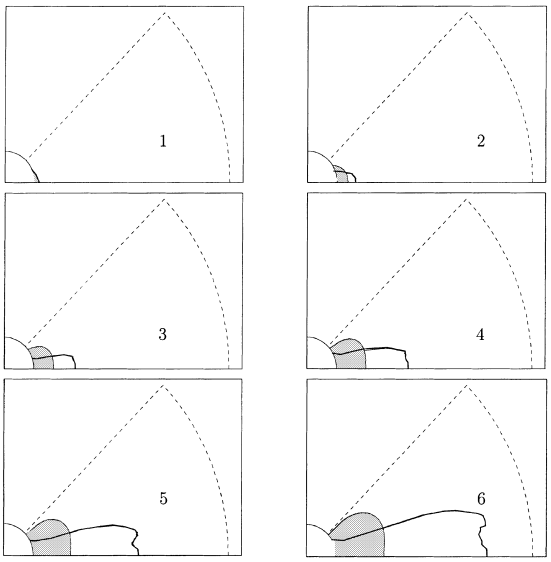

Fig. 13. Development of the craze zone with increasing load at $T = 333$ K for a traction rate of $\dot{p} = 5.52$ MPa/s. The region shown is the full width of the plate (cf. Fig. 9(b)) with the dashed lines indicating the region with cohesive surfaces. The numbered snapshots correspond with the instants shown in Fig. 14. The filled regions represent the zones within which crazing would have initiated according to criterion (6) on the basis of the purely elastic stress state.

the craze widening process. As a consequence, the corresponding overall stress–strain curve, shown in Fig. 14, is practically linear. It is only after the instant #6, where the craze zone has extended until about 75% of the width of the plate, and when crazes would start to breakdown that the crazing would become noticeable in the overall response. This last stage of the process would involve very rapid expansion of the craze zone over the entire width of the plate. To avoid excessively long computing times we did not continue our computations to this stage. However, the elastic prediction of the craze zone shown in Fig. 15 already indicates how quickly this proceeds during the last 10% before the final load.

Finally, we have checked whether the development of the craze zone depends on the finite element mesh size. The development of the craze zone is given in Fig. 16 for the fine mesh used in all previous calculations and a coarse mesh with half the number of cohesive surface elements in radial and circumferential direction. For two values of the global stress level p it is shown that the development of the craze zone is nearly the same for both meshes indicating that mesh refinement leads to a converged craze zone development. Although mesh orientation effects cannot be ruled out completely, considering the shape of the craze zone and noting that crazes form continuously from the boundary of the hole, it is expected that in the current application mesh orientation effects at least do not dominate the solution. A thorough investigation of mesh orientation effects however is beyond the scope of this work, but will be the subject of a forthcoming paper.

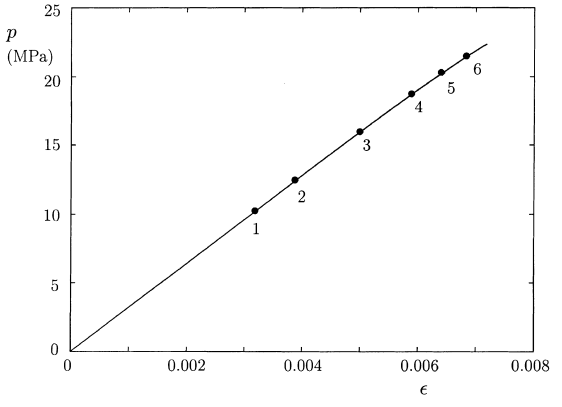

Fig. 14. Global stress p vs strain $\epsilon = \Delta h/h$ curve at $T = 333$ K for a traction rate of $\dot{p} = 5.52$ MPa/s. The numbered data points correspond to the numbers in Fig. 13.

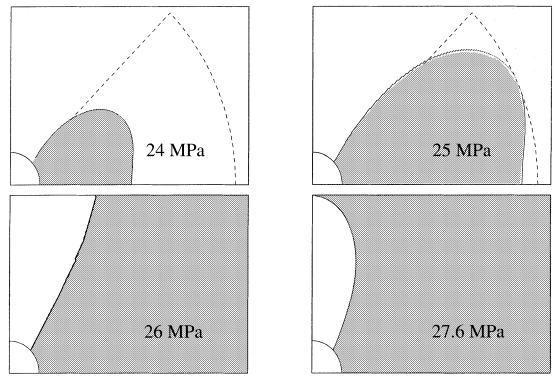

Fig. 15. Development of the zone within which crazing would have initiated according to criterion (6) on the basis of the purely elastic stress state near the final global stress level.

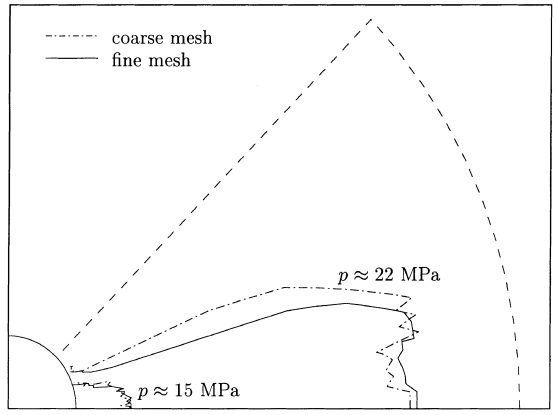

Fig. 16. Craze zone development for the fine mesh of Fig. 9 and a two times coarser mesh for two values of the globally applied stress p for the case with $\dot{p} = 5.52$ MPa/s at $T = 333$ K.

5. Concluding remarks

In this paper we present a new cohesive surface model which describes crazing in amorphous

polymers. Motivated by micromechanical considerations, the model accounts for initiation, widening and breakdown of the crazes. The interaction between continuum description and craze parameters determines the development of the craze zone and no separate model for craze front propagation is used. Using realistic values of the material parameters involved, the model predicts trends in crazing behavior as a function of loading rate or temperature that are consistent with common experimental observations.

The phenomena that are accounted for in the description of crazing include initiation, widening and breakdown of the craze. Unfortunately, the theoretical framework on initiation and breakdown of crazes is still not complete. Important issues like rate effects during craze initiation, the tangential stiffness of a craze and its influence on craze breakdown are still not fully understood. The current model therefore uses the rate independent, stress-dependent craze initiation criterion given by Sternstein et al. (1968). With respect to breakdown of the craze the current model follows experimental results obtained by Döll et al. (1980), though improved understanding has been obtained by the work of Brown (1991), Hui et al. (1992) and Sha et al. (1997) on the important role of the cross-tie fibrils. The cohesive surface methodology is flexible enough to incorporate improved models on initiation and breakdown once these become available.

A key difference with respect to earlier models is that the proposed model incorporates the aspect of rate-dependent deformation through a viscoplastic craze widening law. The description of this process within the cohesive surface context is of vital importance for the final outcome of the analysis, since the redistribution of the continuum stresses is a direct outcome of the softening behavior described by the cohesive surfaces. The continuum stresses will determine the subsequent initiation in other cohesive surfaces, thus describing the propagation of the craze tip. The craze tip velocity is thus a direct consequence of the description of the widening process of the craze material.

The finite element implementation involves separate discretizations of the continuum and the cohesive surfaces and the use of a large number of cohesive surfaces immersed in the continuum to incorporate sufficient freedom for crazes to develop. This allows, in principle, to simulate diffuse as well as highly localized crazing where the location of crazing is not known a priori. The application presented in this paper shows that the model is capable of capturing in a qualitative sense, the rate and temperature dependence of craze development, i.e., the polymer appears more brittle as the temperature decreases or the loading rate increases. Finally, we show that the finite element results for these kind of calculations converge and do not suffer from mesh dependency.

References

Argon, A.S., 1973a. A theory for the low-temperature plastic deformation of glassy polymers. Philos. Mag. 28, 839–865.

Argon, A.S., 1973b. Physical basis of distortional and dilational plastic flow in glassy polymers. J. Macromol. Sci. Phys. B 8, 573–596.

Argon, A.S., Hannoosh, J.G., 1977. Initiation of crazes in polystyrene. Philos. Mag. 36, 1195–1216.

Argon, A.S., Salama, M.M., 1977. Growth of crazes in glassy polymers. Philos. Mag. 36, 1217–1234.

Arruda, E.M., Boyce, M.C., Jayachandran, R., 1995. Effects of strain rate, temperature and thermomechanical coupling on the finite strain deformation of glassy polymers. Mech. Mat. 19, 193–212.

Brown, H.R., 1991. A molecular interpretation of the toughness of glassy polymers. Macromolecules 24, 2752–2756.

Döll, W., Schinker, M.G., Könczöl, L., 1979. A time independent fracture criterion for PMMA. Int. J. Fracture 15, R145–R149.

Döll, W., Seidelmann, U., Könczöl, L., 1980. On the validity of the Dugdale model for craze zones at crack tips in PMMA. J. Mater. Sci. 15, 2389–2394.

Donald, A.M., Kramer, E.J., 1981. The mechanism for craze-tip advance in glassy polymers. Philos. Mag. A 43, 857–870.

Han, H.Z.Y. et al., 1998. Experimental and theoretical studies of the molecular motions in polymer Crazing. Macromolecules 31, 1348–1357.

Hui, C.Y., Ruina, A., Creton, C., Kramer, E.J., 1992. Micromechanics of crack growth into a craze in a polymer glass. Macromolecules 25, 3948–3955.

Kausch, H.H., 1987. Polymer Fracture, Second edition, Springer, Berlin, p. 305.

Knauss, W.G., 1993. Time-dependent fracture and cohesive zones. J. Eng. Mat. Tech. 115, 262–267.

Kotoul, M., 1996. Micromechanical and thermodynamical aspects of environmental crazing. J. Mater. Sci. 31, 3333–3347.

Kramer, E.J., 1983. Microscopic and molecular fundamentals of crazing. Adv. Polymer Sci. 52/53, 1–56.

Kramer, E.J., Berger, L.L., 1990. Fundamental processes of craze growth and fracture. Adv. Polymer Sci. 91/92, 1–68.

Leonov, A.I., Brown, H.R., 1992. A Model of fibril deformation in crazes. J. Polym. Sci. B 29, 197–209.

Peirce, D., Shih, C.F., Needleman, A., 1984. A tangent modulus method for rate-dependent solids. Comput. Struct. 18, 875–887.

Schellekens, J.C.J., De Borst, R., 1993. On the numerical integration of interface elements. Int. J. Num. Meth. Eng. 36, 43–66.

Sha, Y., Hui, C.Y., Ruina, A., Kramer, E.J., 1997. Detailed simulation of craze fibril failure at a crack tip in a glassy polymer. Acta Mater. 45, 3555–3563.

Spiegelberg, S.H., Argon, A.S., Cohen, R.E., 1991. Measurements of craze velocities in polystyrene–polybutadiene blends. J. Appl. Polymer Sci. 48, 85–97.

Sternstein, S.S., Myers, F.A., 1973. Yielding of glassy polymers in the second quadrant of principal stress space. J. Macromol. Sci. Phys. B 8, 539–571.

Sternstein, S.S., Ongchin, L., Silverman, A., 1968. Inhomogeneous deformation and yielding of glasslike high polymers. Appl. Polym. Symp. 7, 175–199.

Telenkov, S.A. et al., 1998. Infrared imaging of stress-crazing in rubber modified polystyrene. Polym. Eng. Sci. 38, 385–391.

Timoshenko, S., Goodier, J.N., 1951. Theory of Elasticity. McGraw-Hill, New York, pp. 80–81.

Van der Giessen, E., Lai, J., 1997. A numerical study of craze growth. In: Deformation, Yield and Fracture of Polymers, vol. 10. The Institute of Materials, London, pp. 35–38.

Van der Giessen, E., Tvergaard, V., 1989. A creep rupture model accounting for cavitation at sliding grain boundaries. Int. J. Fracture 48, 153–178.

Warren, W.E., 1989. On the accuracy of the calculated stress field around a craze. Polym. Eng. Sci. 29, 426–431.

Xiao, F., Curtin, W.A., 1995. Numerical investigation of polymer craze growth and fracture. Macromolecules 28, 1654–1660.

Xu, X.-P., Needleman, A., 1994. Numerical simulations of fast crack growth in brittle solids. J. Mech. Phys. Solids 42, 1397–1434.